Ocean effects on tropical cyclone intensification and inner-core asymmetries

Hongyan Zhu*, Wolfgang Ulrich and Roger K. Smith

Meteorological Institute, University of Munich, Munich, Germany

April 16, 2003

* Corresponding author: Dr. Hongyan Zhu, Meteorological Institute, University of Munich, Theresienstr. 37, 80333 Munich, Germany. Email: hongyan@meteo.physik.uni-muenchen.de

Abstract

The interaction between a tropical cyclone and the ocean is investigated using a minimal three-dimensional tropical-cyclone model coupled with a two-layer ocean model. Two representations for entrainment into the ocean mixed layer are compared: one based on the assumption that the velocity scale for entrainment is the surface friction velocity, the other on the assumption that this scale is the magnitude of the mean velocity difference across the base of the mixed layer.

On a $\beta-$plane with no background flow, the model cyclone moves towards the northwest. With ocean coupling, it leaves a cold wake behind it, mostly to the right of its track. The cooling reduces the heat flux from the ocean and thereby the moist static energy in the boundary layer. As a result, the cyclone is less intense in the mature stage than in the case without cooling.

The magnitude and distribution of the cooling depends strongly on the method for representing entrainment. The method based on the surface friction velocity is more effective in reducing the heat flux from the ocean to the storm under the core region and leads to a greater reduction of the tropical cyclone intensity.

With ocean coupling, the surface heat flux is reduced, mainly in the rear-right quadrant of the cyclone core. As a result, the potential temperature distribution in the core region is more asymmetric in the coupled model, with a higher value in the northern sector than in the south sector. The region of convergence in the lower troposphere in the coupled experiments is rotated counterclockwise from the rear quadrant of inner core to the eastern quadrant, apparently in response to the change in the distribution of the potential temperature. In addition, the region of strong upward motion in the middle troposphere shifts from the rear-right quadrant to the front-right quadrant. These changes are accompanied mainly with changes in the divergence pattern in the lower troposphere rather than in the boundary layer.

1. INTRODUCTION

To a first approximation the mature hurricane can be thought of as a Carnot heat engine that extracts energy from the ocean at the sea surface temperature (SST) and loses it in the form of infrared radiation to space at a temperature close to that of the tropopause (Emanuel, 1986). In general the local rate of supply of heat energy (primarily latent heat) from the ocean increases with increasing surface wind speed, but is limited by the degree of thermal disequilibrium between the atmosphere and the ocean, which increases strongly with increasing SST and with decreasing surface pressure. As a storm intensifies, the increasing surface wind speeds and decreasing pressures lead to increased surface heat fluxes, which feed back through the vortex dynamics to further increase the surface winds (this is the so-called WISHE*-theory of hurricane intensification proposed by Emanuel, 1989). However, the increasing surface wind stress also generates ocean currents and strong turbulent mixing in the ocean. The mixing deepens the ocean mixed layer, entraining cooler thermocline water into it, which in turn lowers the SST. Observations show that the maximum SST reduction lies between 1 and 6^oC, depending on the translation speed of the cyclone (Black, 1983). The cooling reduces the degree of thermal disequilibrium across the air-sea interface or may even reverse the heat and moisture fluxes across the interface so that intensification ceases or the hurricane begins to decay. In this way, the ocean can have a negative feedback on hurricane intensification.

Ocean mixed layer modelling began at the end of 60's with the development of one-dimensional models (e.g. Kraus and Turner 1967, Niiler and Kraus 1977). During the 70's, two- and three-dimensional ocean models were designed to investigate the response of the ocean to the specified surface stresses imposed by hurricanes (e.g. Geisler 1970, Elsberry *et al.* 1976, Chang and Anthes 1978, Price 1981). Chang and Anthes (1978) used a three-dimensional ocean model to investigate the oceanic response to moving hurricane. They used a turbulent kinetic energy budget to determine the stress-induced vertical mixing and related the entrainment of thermocline water into the mixed layer to the surface friction velocity. Price (1981) carried out a similar study, but related the entrainment to the mean horizontal velocity difference across the base of the mixed layer.

The earliest simulations of the *coupled* hurricane-ocean system were performed by Chang and Anthes (1979) and Sutyrin *et al.* (1979) using axisymmetric hurricane and ocean models with a relatively coarse horizontal resolution. Their calculations suggested that the effects of sea surface cooling on hurricane intensification is small. In contrast, Ginis *et al.* (1989) coupled a three-dimensional, five-level hurricane model with a three-layer primitive equation ocean model and showed that the sea surface cooling has a significant effect on the intensification and as well as the cyclone speed. Bender *et al.* (1993) performed a set of idealized numerical experiments using a high-resolution coupled hurricane ocean model. Calculations were performed in which a tropical cyclone vortex was embedded in uniform easterly or westerly basic flows of different strengths. They found that slower-moving storms produced a progressively larger SST response, a greater decrease of the total heat flux, and hence suffered a larger reduction in intensity than faster-moving storms.

* WISHE is an acronym for Wind-Induced Surface Heat Exchange coined by Yano and Emanuel (1991)

Recently Schade and Emanuel (1999) carried a parameter study using an axisymmetric hurricane model (Emanuel, 1989) coupled with a three-layer ocean model. The hurricane model is formulated using potential-radius coordinates†, in which the radial resolution in physical space is high in regions where the radial gradient of angular momentum is large. In some of their calculations, the SST feedback effect reduces the hurricane's intensity by more than 50%.

Chan *et al.* (2001) coupled MM4 (The fourth-generation National Center for Atmospheric Research/Penn State University Mesoscale Model) with a simple ocean model to explore the evolution of intensity and structure of a hurricane in different ocean configurations, including the presence of a warm pool or large SST gradients. They found, *inter alia*, that changes in storm intensity are not only sensitive to the SST, but also to the initial depth of the ocean mixed layer and to the vertical structure of ocean. In presence of a warm core eddy, the tropical cyclone intensifies prior to reaching the centre of the eddy.

There may be limitations of using an axisymmetric hurricane model as part of a coupled model if the ocean response is highly asymmetric about the moving storm centre, especially on the scale of the inner core. The extent to which this might be the case is examined this paper using a minimal three-dimensional hurricane model (Zhu and Smith, 2003) coupled with a simple two-layer ocean model. Two choices for the entrainment parameterization of the ocean mixed layer, based on the models of Chang *et al.* (1978) and Price (1981) are compared, and the sensitivity of the hurricane intensity and structure to the different entrainment laws is explored. We investigate also the modified asymmetric structure in the inner core region of hurricane caused by the SST cooling. A brief description of the tropical cyclone and ocean models is presented in section 2. The response of the ocean to the moving hurricane is discussed briefly in section 3, while the impact of ocean on the hurricane is analyzed in detain in section 4. A summary of the results and conclusion is presented in section 5.

2. The coupled model

(*a*) *Hurricane model*

The hurricane model is that described in Zhu and Smith (2003, henceforth referred to as ZS). It is three-dimensional and based on the hydrostatic primitive equations formulated in σ-coordinates (x, y, σ) on a β-plane. It uses the Charney-Phillips grid (CP-grid) for the vertical differencing (see Fig.1). The model equations and the advantages of CP-grid are discussed in ZS. The model is divided vertically into four layers of unequal depth in σ: the lowest layer has depth 0.1 and the three layers above have depth 0.3. Newtonian cooling is used to represent the effect of radiative cooling. The turbulent flux of momentum to the sea surface and the fluxes of sensible heat and water vapour from the

† Potential radius is the radius to which an air parcel must be moved (conserving absolute angular momentum) in order to change its tangential velocity component to zero. It is proportional to the square root of the absolute angular momentum per unit mass about the storm centre.

surface are represented by bulk aerodynamic formulae. The surface drag coefficient, C_D, is calculated from the formula used by Shapiro (1992):

$$C_D = (1.024 + 0.05366 R_F \, |\mathbf{u_b}|) \times 10^{-3}, \tag{1}$$

where $R_F = 0.8$ is used to reduce the boundary layer wind, $\mathbf{u_b}$ to the 10-m level. The surface exchange coefficients for moisture and heat are assumed to be equal to each other and to C_D. The consequences of allowing these quantities to differ are investigated by Emanuel (1995).

Explicit condensation occurs when the air becomes supersaturated at a grid point. At such points the excess water is assumed to precipitate out while the latent heat released increases the air temperature. The scheme, which is described in detail by Zhu *et al.*, (2001; henceforth referred to as ZSU), involves an iterative procedure.

The parameterization of deep cumulus convection is based on a mass flux approach suggested by Arakawa (1969) and detailed in Zhu *et al.*, (2001; henceforth referred to as ZSU). Implementation of the scheme in the present CP-grid formulation requires that the subgrid-scale mass fluxes associated with deep convection be offset vertically on the grid compared with those on the resolved scale, in contrast to the representation of the scheme in the Lorenz-grid used by ZSU, while this is conceptually inelegant because the grid-scale average of the vertical motion at any height must be equal to the resolved scale vertical motion, the effects of sub-grid scale and resolved scale vertical motion on the temperature and moisture tendencies are simply additive and can be calculated separately, as, indeed, they are in the Lorenz-grid formulation described in ZSU. A schematic diagram of the flow configuration in a grid box is shown in Fig. 1. It incorporates a steady bulk cloud model for deep convection in which M_{c3} is the cloud-base mass flux from the top of the boundary layer (level-$3\frac{1}{2}$) to the cloud, M_e is the mass flux entrained at level-$2\frac{1}{2}$ into the cloud, and M_{c2} is the mass flux that detrains at the upper level-$1\frac{1}{2}$. The entrainment rate, M_e, is determined by solving equations for mass and energy conservation. The precipitation downdraft mass flux is related to the updraft mass flux by the precipitation efficiency (see ZSU). A closure assumption is required in the convection scheme to determine M_{c3}. As suggested by Arakawa (1969), it is assumed that deep convection tends to reduce the conditional instability on the time-scale τ_{dc} (1 h). The details of the equations are given in ZSU.

(*b*) *Ocean model*

The ocean model has two layers: a well-mixed layer, in which the density and horizontal velocity are independent of depth, and an infinitely deep layer, which is at rest. The sea surface is treated as a rigid lid to exclude the barotropic mode.

The momentum balance of the mixed layer in Cartesian coordinates, similar to Chang and Anthes (1979, henceforth referred to as CA), is

$$\frac{\partial u}{\partial t} = -\left(u\frac{\partial u}{\partial x} + v\frac{\partial u}{\partial y}\right) - \left(\frac{1}{2}gh\frac{\partial \epsilon}{\partial x} + \epsilon g\frac{\partial h}{\partial x}\right) + fv + \frac{\tau_x}{\rho h} + K_m \nabla^2 u + \left(\frac{du}{dt}\right)_m \tag{2}$$

$$\frac{\partial v}{\partial t} = -\left(u\frac{\partial v}{\partial x} + v\frac{\partial v}{\partial y}\right) - \left(\frac{1}{2}gh\frac{\partial \epsilon}{\partial y} + \epsilon g\frac{\partial h}{\partial y}\right) - fu + \frac{\tau_y}{\rho h} + K_m \nabla^2 v + \left(\frac{dv}{dt}\right)_m \tag{3}$$

where u and v are the velocity components in the x- and y-directions, $f = f_o + \beta y$ is the Coriolis parameter, f_o and $\beta = df/dy$ are constants, h is the mixed layer depth, g is the acceleration due to gravity, and ρ is the mixed layer density. The terms on the right side of Eq. 2 and Eq. 3 represent horizontal advection, the pressure gradient force, Coriolis force, the acceleration due to the wind stress, horizontal diffusion and the acceleration due to the vertical mixing of the momentum, respectively. As in CA, the density anomaly ϵ is given by

$$\epsilon = \frac{\rho_b - \rho_m}{\rho_b} = \alpha(T - T_b) \tag{4}$$

where ρ_m and ρ_b are the densities of the mixed layer and bottom layer, respectively, T is the temperature of the mixed later, T_b is the temperature of the deep ocean, and α is the expansion coefficient of water near 20 C^o (about 2×10^{-4}). The stress field is defined by $\tau = C_d \rho \vec{V_{air}} |\vec{V_{air}}|$, where the drag coefficient C_D is given by Eq. 1.

The thermodynamic equation is

$$\frac{\partial T}{\partial t} = -\left(u\frac{\partial T}{\partial x} + v\frac{\partial T}{\partial y}\right) + K_m \nabla^2 T + \left(\frac{dT}{dt}\right)_m \tag{5}$$

where the terms on the right-hand-side represent advection, horizontal diffusion, and the effect of the vertical mixing with deep ocean water, respectively.

The depth of the mixed layer is predicted by the equation of continuity

$$\frac{\partial h}{\partial t} = -\left(u\frac{\partial h}{\partial x} + v\frac{\partial h}{\partial y}\right) + \left(\frac{dh}{dt}\right)_m \tag{6}$$

where the terms on the right represent the effects of horizontal divergence and vertical mixing.

Following Price (1981), the contributions due to vertical mixing in the west-east and south-north directions are defined as follows,

$$\left(\frac{d\chi}{dt}\right)_m = \frac{\delta\chi}{h}\omega_e \tag{7}$$

$$\left(\frac{dh}{dt}\right)_m = \omega_e \tag{8}$$

where ω_e is the entrainment velocity and $\delta\chi$ is one of the quantities: $\delta u = u_b - u_m$, $\delta v = v_b - v_m$, or $\delta T = T_b - T_m$.

Mixed layer deepening is fundamentally a turbulent process (Phillips, 1977). The mixing velocity (ω_e) and the velocity scale (U) have the following relationship,

$$\frac{\omega_e}{U} = E(R_i) \tag{9}$$

where E is some entrainment function, which needs to be defined, and Ri is the overall Richardson number of the mixed layer, defined as

$$R_i = \frac{g\epsilon h}{U^2}. \tag{10}$$

The velocity scale characterizing entrainment into the oceanic mixed layer is usually assumed to be either the friction velocity characterizing the surface wind stress, $\mathbf{u}_*$, or the magnitude of the mean velocity difference across the base of the mixed layer, $\delta\mathbf{u}$. In this study, we compare these two assumptions. The first choice is the basis of the *turbulent erosion model* (TEM) (Price, 1978), for which the entrainment velocity is given by,

$$\omega_e = \frac{2.5u_*^3}{g\epsilon h} \tag{11}$$

where $u_*^2 = \tau/\rho$. This formulation of entrainment parameterization was investigated by Kato and Phillips (1969) and CA. The second choice for the entrainment velocity forms the basis of the *dynamic instability model* (referred to as DIM by Price, 1978), which holds that the entrainment is associated with shear instability at the bottom of the mixed layer (Pollard *et al.* 1973), The assumption is that the wind stress causes the velocity shear across the bottom of the mixed layer, and the shear instability leads to the turbulent entrainment. This parameterization was formulated by Price (1979), who carried out laboratory experiments on the scaling of stress-driven entrainment. In his formulation, the entrainment velocity is given as,

$$\begin{aligned} \omega_e = &\quad 5 \times 10^{-4} R_v^{-4} \delta\mathbf{u}, \quad 0 \le R_v \le 1 \\ = &\quad 0, \qquad\qquad\quad R_v > 1 \end{aligned} \tag{12}$$

where $\delta\mathbf{u}$ is the mean velocity difference at the base of the mixed layer, and R_v is the bulk Richardson number defined by,

$$R_v = \frac{g\epsilon h}{(\delta\mathbf{u})^2} \tag{13}$$

(*c*) *Initial condition*

The initial vortex is axisymmetric and barotropic, with the tangential wind profile used by Smith *et al.* (1990), but with different parameters: the maximum tangential wind speed is 20 m s^{-1} at a radius of 180 km. The initial mass and thermal fields are obtained by solving the inverse balance equation (see ZSU). The far-field temperature, geopotential height and humidity structure are based on the mean West Indies sounding (Jordan 1957). The time step for the hurricane model is 12 s. The initial ocean mixed layer thickness is 70 m, the temperature of the mixed layer is 28^{o}C, and the temperature of the deep ocean is 20^{o}C. The dominant periodicity in the ocean response is inertial, suggesting a time step of O(10^3 s) (Price, 1981). For this reason we set the time step for the ocean model to be 900 s.

(*d*) *Experiment design*

The method of coupling the hurricane and the ocean models is carried out as follows. During the period of one ocean model time step, the hurricane model is integrated forward in time keeping the SST constant. The wind stress computed in the hurricane model is then passed to the ocean model. The ocean model is integrated for one time step and a

new SST is calculated. Each model run is integrated to 72 h, at which stage the hurricane has achieved a quasi-steady state. Three experiments are carried out as detailed in Table 1. The control experiment (Expt. 1) is an integration of the hurricane model by itself with a uniform SST of 28^{o}C. The second and third experiments are calculations using the coupled model with the entrainment parameterization based on TEM (Expt. 2) or DIM (Expt. 3).

3. Ocean response

The patterns of storm-induced ocean cooling in Expts. 2 and 3 after 72 h of integration are displayed in Fig. 2. In each case there is pronounced cooling to the right of the hurricane track. Previous studies have shown that the entrainment into the mixed layer is the major cause of this cooling (i.e. CA, Price 1981, Shay *et al.* 1992, Bender 1993, and Chan *et al.* 2001).

There are differences in the magnitude and areal extent of the cooling using different entrainment schemes. In Expt. 2 the maximum cooling is located about 500 km behind the storm centre (Fig. 2a). The cooling directly underneath the hurricane core, which is indicated by the isotachs of surface wind speed 30 m s^{-1} or larger, lies approximately in the range of 0.5^{o}C - 1.5^{o}C and surrounds the hurricane centre, but a noticeable asymmetry exists about the hurricane centre with a right-of-track bias. The cooling on the east of the core reaches over 1.5^{o}C, while on the western side it is less than 1^{o}C. The mixed layer cooling in Expt. 3 (Fig. 2b) covers a narrower region than in Expt. 2, but the magnitude of the cooling is stronger: underneath core region, the reduction in SST reaches nearly 4^{o}C, which is twice that in Expt. 2, and the cooling occurs mainly in the rear-right quadrant of core. Unlike Expt. 2, there no obvious cooling to the left of storm track and ahead of storm centre. Beyond 200 km of the storm centre, the pattern of cooling is similar in the two experiments.

The reasons for the differences in the cooling distributions in the two experiments may be understood in terms of the different formulations for the entrainment velocity at the base of the oceanic mixed layer. In Expt. 3, the entrainment velocity depends on the vertical shear at the base of the mixed layer, and since the deep ocean layer is assumed to be at rest, the entrainment velocity is solely determined by the mixed layer currents, which have a right bias relative to the storm track (Price 1981 and Bender 1993). This asymmetry in the mixed-layer currents introduces a right bias asymmetry in the entrainment, which is mainly responsible for the cooling. Because of the neglect of the current speed in the deep ocean, the entrainment velocity in the DIM formulation may be slightly overestimated. The entrainment velocity in Expt. 2 is proportional to the friction velocity induced by the surface wind. In this case, the distribution of mixed layer entrainment is similar to that of the surface wind speed, which is strongest to the right of the hurricane track (Shapiro, 1983).

Recently Jacob and Shay (2003) investigated the ocean mixed layer response to Hurricane Gilbert (1988) in the western Gulf of Mexico, and compared four parameterizations for entrainment into the ocean mixed layer. They found similar results to those shown here. In their simulations, the entrainment schemes based on the shear of ocean currents

predict intense entrainment due to enhanced shears near the storm track with the entrainment mixing confined to a narrower region compared with the schemes in which the entrainment velocity is partly proportional to the surface friction velocity. Also a deeper and cooler mixed layer occurs to the left of the storm track in latter cases compared with little entrainment and cooling in the former cases.

As the ocean response to a moving hurricane has been explored by many previous workers, we focus here mainly on the hurricane response to the ocean cooling. The effects of mixed-layer cooling on the intensification and structure of the tropical cyclone in the two experiments are discussed in the next section.

4. Hurricane response

(*a*) *Changes in hurricane intensity*

The time evolutions of the minimum surface pressure and maximum boundary layer wind speed of the hurricane in Expts. 1-3 are compared in Fig. 3. During the gestation period, when the model hurricanes are slowly intensifying, the intensification rates in the three calculations are almost identical. Small differences emerge after 20 h of integration during the period of rapid intensification, but these difference remain small until the vortex reaches the mature stage, at about 30 h, when the wind speed in each experiment reaches a maximum. The mean storm intensity during the mature stage, beyond 36 h, is lower in the coupled model runs compared with that in the control experiment. At 72 h, for example, the minimum surface pressure is 980 mb in the control calculation compared with 990 mb in Expt. 2 and 988 mb in Expt. 3. The corresponding maximum boundary layer wind speeds at this time are about 50 m s^{-1}, 38 m s^{-1} and 40 m s^{-1}, respectively.

In an approximate steady-state theory for a hurricane that assumes neutrality to slantwise convection throughout the vortex, Emanuel (1986) derived the relationship $\Delta p = -3.3\Delta\theta_e$ between the difference in the reversibly-defined equivalent potential temperature $\Delta\theta_e$ between the outer periphery of the storm and its centre, and the difference in the mean sea level pressure Δp over this region. The increase in θ_e, or equivalently in the moist static energy* H, arises mainly because of the greatly enhanced latent heat fluxes in the region of strong surface winds and low pressures surrounding the storm centre. Numerical model calculations for real storms by Bender and Ginis (2000) indicate some variability in the ratio $-\Delta p/\Delta\theta_e$ with values lying between 3.1 and 4.2, but the two studies highlight the relationship between vortex intensity as measured by Δp and the elevation of θ_e (or equivalently ΔH) near the vortex centre. It is therefore of interest to examine the effects of ocean coupling on the distributions of surface heat flux and boundary-layer moist static energy in our model.

We have shown above that even though the mixed-layer cooling in the hurricane core region is larger in Expt. 3 than in Expt. 2, it occurs mainly in the rear-right quadrant, while in Expt. 2 cooling occurs over the whole inner core area. As a result, the cooling

* The moist static energy is defined by the formula $H = c_pT + Lq + \Phi$, where c_p is the specific heat of dry air, T is the temperature, q is the specific humidity and Φ is the geopotential height.

might be more effective in reducing the total heat flux from the ocean to the atmosphere in Expt. 2. To investigate this possibility we show the distributions of total heat flux at 72 h in the three experiments (Fig. 4). The total heat flux from the ocean in the control experiment is positive in the inner core region (Fig. 4a) with a maximum in the front-right quadrant, consistent with the distribution of the maximum boundary layer wind speed. The maximum value is around 0.24 kWs^{-1}, and the main contribution to the total heat flux is the latent heat flux, which is about three times the sensible heat flux. In Expt. 2 (Fig. 4b) the total heat flux is reduced in the whole core region compared with Expt. 1. The heat flux is positive in the north and northwest quadrant of the vortex, but the maximum value is only 0.15 kWs^{-1}, about 50% less than that of Expt. 1, and there is a negative heat flux in the south and southeastern quadrant, above the cold wake, with a minimum value of -0.25 kWs^{-1}. In Expt. 3 (Fig. 4c) the total heat flux is reduced mainly in the rear-right part of the core region due to the cooling, and the minimum value is -0.7 kWs^{-1}. The total heat flux to the north and west of the core in Expt. 3 is positive and the maximum is 0.5 kWs^{-1} in the front-right of the core region, much higher than that in Expt. 2.

The azimuthally-averaged total heat flux at 72 h in the three experiments is compared in Fig. 5. As expected from Fig. 5, the average flux in the vortex core region is strongest in Expt. 1 where the ocean cooling is not included. In Expt. 3, the average flux is less than that in Expt. 1, but is still positive. The average flux in Expt. 2 is much less than in the control experiment, and it is slightly negative at a radius of 80 km. The average flux is larger in Expt. 3 than in Expt. 2 because the mixed-layer cooling occurs only in a small fraction of the vortex core region instead of covering the whole area of the core as in Expt. 2.

A reduction of the surface heat flux from ocean to the vortex diminishes the moist static energy not only in the boundary layer, but also above the boundary layer where there is ascent out of the boundary layer. This is clear from Fig. 6, which compares the azimuthally-averaged moist static energy at the level above the boundary layer (-level $3\frac{1}{2}$) in Expts. 1-3. At 72 h, the maximum value is about 362 kJ kg^{-1} in the central region of the vortex in Expt. 1, whereas in Expt. 2 this value is reduced to 355 kJ kg^{-1} and in Expt. 3 to 357 kJ kg^{-1}. The result is significant, because the radial buoyancy gradient in the inner core of a mature hurricane is determined mainly by that of moist static energy in the boundary layer (Smith, 2003). It is interesting to note that Expt. 1 has the largest radial gradient of moist static energy, and Expt. 2 has the smallest radial gradient. At 72 h, the stronger radial gradient of moist static energy is associated with a more intense vortex. We hypothesize that during the intensification phase of the model hurricane, a stronger buoyancy gradient above the boundary layer leads to stronger convergence there and therefore to the spin up of a more intense hurricane. Our calculations show that the cooling of the ocean reduces the surface heat flux to the atmosphere and thereby the moist static energy and its radial gradient in the boundary layer, and to a weaker hurricane.

(*b*) *Modification of asymmetry in the inner core region*

Bender (1997) investigated the asymmetries that develop in the Geophysical Fluid Dynamics Laboratory high-resolution hurricane model with a fixed SST, which includes

a parameterization of deep convection. A vorticity analysis in a variable-f experiment in an otherwise quiescent environment suggested that large asymmetries in the storm's interior are a consequence of the vertical shear of the beta-gyre flow. The shear arises because of the decrease of the storm's cyclonic circulation with height above the boundary layer, which reduces the strength of the gyres. The analysis indicates that quasi-steady asymmetries in the inner core region are a result of vorticity advection differences between the beta gyre flow in the lower free atmosphere and the storm motion. The resulting low level inflow through the vortex from the southeast, which is a maximum at a height of about 1.3 km (see Bender's Fig. 4) advects the symmetric vorticity and leads to a large positive vorticity tendency ahead of the centre and a large negative tendency behind. Bender's analysis indicates that these tendencies are balanced by areas of divergence and vorticity compression ahead of the storm and enhanced convergence and vorticity stretching behind the vortex (see Bender's Figs. 5 and 6), which in turn are associated with large asymmetries in the vertical motion in the middle troposphere and accumulated precipitation, with maxima in these two fields occurring in the rear of the vortex core region (see Bender's Fig. 7). While this analysis does not provide a complete explanation for the mechanism producing the asymmetries, as it does not give a dynamical reason for the diagnosed pattern of asymmetric divergence, it does point to the important role of the shear.

The effect of vertical shear on the dynamics of even a dry vortex is rather complicated and the shear is known to produce significant asymmetries in the flow (see e.g. Jones, 1995, 2000a, 2000b; Frank and Ritchie, 1999; and references therein). Unlike Bender's study, all these investigations relate to calculations performed on an f-plane. An succinct review of the mechanisms involved in producing the asymmetries is given by Jones (2003). Frank and Ritchie (1999, 2001) investigated the additional effects of moist processes on the shear-induced asymmetries using MM5. Frank and Ritchie (1999) used a model configuration with that included both explicit and parameterized schemes for moist deep convection and concluded that the pattern of convection in the storm's core is strongly influenced by vertical wind shear, to a degree comparable with the influence of boundary layer friction. Their model simulations with moist processes included show strong upward motion and rainfall on the downshear left side of the vortex, different from the dry simulations where the strong upward motion is on the downshear right. They argue that in the moist runs the component of the secondary circulation forced by vertical shear is due to the direct effects of differential vorticity advection upon a quasi-balanced vortex. Using MM5 with a higher resolution than their earlier study and only an explicit representation of moist processes, Frank and Ritchie (2001) obtained results similar to those in their 1999 paper, and which, in an the easterly shear case, were broadly in line with results presented by Bender (1997). The further investigation of the quasi-steady asymmetries of the interial hurricane in the shear environment will be our future work. All of the foregoing studies were for a fixed SST. Here we examine the effects of a coupled ocean using our model.

Figure 7 shows a plot of the vertical p-velocity field (ω) at the middle level (level-$2\frac{1}{2}$), averaged over the integration period 60 h to 72 h, in Expts. 1-3 when the vortex is in the mature (quasi-steady) stage. In Expt. 1, the strongest upward motion is concentrated in the rear and rear-right of the the vortex centre (panel (a)), broadly similar with the results of Bender (1997; see his Fig. 7 (top)). Panels (b) and (c) of Fig. 7 show the

same time-averaged fields for Expts. 2 and 3 and indicate that the asymmetry is altered considerably when the ocean coupling is included. The pattern of upward motion in these experiments is rotated counterclockwise through an angle of about 90^o compared with that shown in panel (a), so that the largest ascending velocities are shifted to the northern sector of the storm.

To investigate the differences in the vertical velocity asymmetries between the calculations with and without ocean coupling, the divergence fields averaged over the same 12 h period are compared in Fig. 8. Panels of (a) and (b) show the divergence field in the boundary layer (level-4) and in the lower troposphere (level-3) in Expt. 1. In the boundary layer, without ocean coupling, there is convergence throughout the core with a maximum of $-6 \times 10^{-4}\mathrm{s}^{-1}$ located on the front-right side of the vortex track, about 50 km from the vortex centre. This pattern is broadly in agreement with the results of Shapiro (1983), who used a simple slab boundary layer model to analyze the effects of vortex movement on the pattern of frictional convergence in a hurricane-like vortex. In the lower troposphere, at level-3, the divergence has primarily an azimuthal wavenumber-one pattern with a maximum ahead of the vortex, and a minimum (maximum convergence) located at the rear. This is consistent also with Bender's (1997) results (see his Fig. 5 (top)). Comparing Figs. 8a and b, the area of largest divergence in the lower troposphere (level-3) lies approximately above the region of largest frictional convergence in the boundary layer (level-4). As explained by Bender (1997, Fig. 6 (top)), the region of large ascent associated with the boundary layer convergence in the front of the core region does not extend to large heights because of the asymmetric divergence above, and, in fact, the largest ascending motion at the middle level in Expt. 1 is located in the rear quadrant of the vortex core.

When the ocean coupling is included, the divergence pattern in the lower troposphere (level-3) has a rather different structure, although there is little change in the boundary layer (level-4) (cf. panels (c) and (d) of Fig. 8 with panels (a) and (b), respectively). The patterns are similar in the boundary layer because in both cases the vortices are moving in a northwesterly direction (the differences in the track introduced by the ocean cooling are very small as shown in Fig. 10). The maximum ascent out of the boundary layer (figures not shown) is located in the front-right quadrant of the core in all three experiments, consistent with the distribution of the maximum convergence in the boundary layer. The differences in the asymmetries of vertical velocity in the middle troposphere (level-$2\frac{1}{2}$) in Fig. 7 between the experiments with and without ocean coupling are associated mainly with the differences in the pattern of the divergence in the lower troposphere (level-3). In Expt. 2, where ocean coupling is included, the centres of maximum convergence and divergence are rotated counterclockwise through about 45^o (cf. panel (d) with panel (b) in Fig. 8), with the maximum divergence to the west and maximum convergence to the east of the centre. Compared with Expt. 1, the absolute values of the maximum convergence and divergence in Expt. 2 are reduced from $0.8 \times 10^{-4}\mathrm{s}^{-1}$ to $0.3 \times 10^{-4}\mathrm{s}^{-1}$ and there is now a region of weak convergence in front of the vortex instead of divergence. Therefore, in this case, the area of divergence in the lower troposphere is weaker and doesn't overlie the region of boundary layer convergence. In this case the maximum ascent in the middle troposphere approximately coincides with the maximum convergence in the boundary layer.

It is reasonable to presume that the changes in the divergence pattern in the lower troposphere in panels (b) and (d) of Fig. 8 are related to the differences of the surface heat flux in the Expt. 1 and Expt. 2 (see Fig. 4a, b). As discussed earlier, the ocean cooling in the vortex core region in Expt. 2 occurs mainly in the rear quadrant, where it leads to a negative heat flux. The effect of the reduced heat flux on the vortex itself is evident in the potential temperature asymmetry at the middle level (level-$2\frac{1}{2}$), averaged over the same 12 h period as in Fig. 7. This field is shown in Fig. 9 for Expts. 1 and 2. In both experiments, there is positive potential temperature anomaly in the northern sector of the core region and a negative anomaly in the southern sector, consistent with the maximum surface heat flux lying in the front-right quadrant in both cases (Fig. 4a, b). The major difference between the two experiments is that the absolute values of the positive and negative centres of the potential temperature asymmetry are much larger in Expt. 2 compared with Expt. 1: thus the potential temperature field is more asymmetric in the coupled experiment, with a higher value to the north of the centre. Since areas of enhanced potential temperature are regions of enhanced buoyancy, we would expected them to produce regions of increased horizontal convergence. We hypothesize that in Expt. 2, the positive heat flux in the front and front-right quadrant accounts for the increased convergence ahead of the storm in the lower troposphere and likewise the negative heat flux to the rear of the storm reduces the convergence.

The inner core asymmetries in Expt. 3 (Fig. 7c) are similar to those in Expt. 2. For the same reason as Expt. 2 (figures not shown), the asymmetric pattern of ocean cooling reduces the heat flux in the rear quadrant of the vortex core and introduces a shift in the maximum ascent from the rear-right of the vortex to the front-right.

5. Conclusion

Calculations performed with a simple coupled hurricane-ocean model show that a moving hurricane produces a cold wake in the ocean with the maximum cooling to the right of the track, consistent with other studies. The cooling leads to a reduction of the heat flux from the ocean, which, in turn, diminishes the moist static energy in the boundary layer leading to a less intense mature hurricane.

The magnitude and the distribution of the cooling is different in experiments with different parameterizations for mixing in the oceanic mixed layer. In the experiment with the turbulent erosion model for mixing, cooling occurs on the periphery of the storm core with the strongest cooling to the right of the vortex track. In contrast, with the dynamic instability model for mixing, the cooling occurs only in the rear quadrant of the storm. It turns out that the turbulent erosion model is more effective in reducing the heat flux from the ocean to the storm under the core region, causing a greater reduction of the storm intensity. At the time of writing we are not in a position to say which of these mixing hypotheses is the more realistic.

Without ocean coupling, a moving hurricane on a β-plane exhibits quasi-steady asymmetries in the core region with a persistent area of divergence in the lower troposphere ahead of the vortex and an area of convergence to the rear. The region of divergence overlays that where the frictional convergence in the boundary layer is largest. As a result, the largest ascent in the middle troposphere occurs in the rear quadrant of the core.

With ocean coupling, the surface heat flux is reduced mainly in the rear-right quadrant of the core and the corresponding potential temperature distribution in the troposphere has much higher value in the northern part of the core compared with the southern part. For this reason the pattern of convergence in the lower troposphere is different in the coupled experiments with convergence in the front right part of the core instead of divergence. The corresponding maximum vertical velocity coincides with the region of frictional convergence in the boundary layer and is located in the front right of the inner core.

Acknowledgements

This work was supported by the US Office of Naval Research through Grant No. N00014-95-1-0394. We are grateful Dr. Lloyd Shapiro for helpful discussions and for his thoughtful comments on an earlier version of this paper.

References

Arakawa, A., 1969: Parameterization of cumulus convection. *Proc. WMO/IUGG Symp. Numerical Weather Prediction, Tokyo, 26 November - 4 December 1968, Japan Meteor. Agency IV*, **8,** 1-6.

Bender, M. A., I. Ginis and Y. Kurihara, 1993: Numerical simulations of tropical cyclone-ocean interaction with a high-resolution coupled model. *J. Geophys. Res.*, **98**, 23245-23263.

Bender, M. A., 1997: The effect of relative flow on the asymmetric structure in the interior of hurricanes, *J. Atmos. Sci.*, **54**, 703-724.

Bender, M. A., and I. Ginis, 2000: Real-case simulations of hurricane-ocean interaction using a high-resolution coupled model: Effects on hurricane intensity , *Mon. Wea. Rev.* **128**, 917-946.

Black, P. G., 1983: Ocean temperature change induced by tropical cyclones, *Ph.D. dissertation, Pennsylvania State University, University Park*, 278.

Chan, J. C. L., Y. Duan, and L. K. Shay, 2001: Tropical cyclone intensity change from a simple ocean-atmosphere coupled model, *J. Atmos. Sci.*, **58**, 154-172.

Chang, S. W., and R. A. Anthes, 1978: Numerical simulations of the ocean's nonlinear baroclinic response to translating hurricane. *J. Phys. Oceanogr.*, **8**, 468-480.

Chang, S. W., and R. A. Anthes, 1979: The mutual response of the tropical cyclone and the ocean, *J. Phys. Oceanogr.*, **9**, 128-135.

Emaunel, K. A., 1986: An air-sea interaction theory for tropical cyclones, Part I: Steady-state maintenance, *J. Atmos. Sci.*, **43**, 585-604.

Emanuel, K. A., 1989: The finite-amplitude nature of tropical cyclogenesis, *J. Atmos. Sci.*, **46**, 3431-3456.

Emaunel, K. A., 1995: Sensitivity of tropical cyclones to surface exchange coefficients and a revised steady state model incorporating eye dynamics, *J. Atmos. Sci.*, **52**, 3969-3976.

Elsberry, R. L., T. Fraim, and R. Trapnell, 1976: A mixed layer model of the oceanic thermal response to hurricanes. ,*J. Geophys. Res.*, **81**, 1153-1162.

Frank, M. W., and E. Ritchie, 1999: Effects of environmental flow upon tropical cyclone structure., *Mon. Wea. Rev.*, **127**, 2044-2061.

Frank, M. W., and E. Ritchie, 2001: Effects of vertical wind shear on the intensity and structure of numerically simulated hurricanes., *Mon. Wea. Rev.*, **129**, 2249-2269.

Geisler, J. E., 1970: Linear theory of the response of a two layer ocean to a moving hurricane., *Geophys. Fluid Dyn.*, **1**, 249-272.

Ginis, I., and Kh. Zh. Dikinov, 1989: Modeling of the Typhoon Virginia (1978) forcing on the ocean. *Sov. Meteorol. and Hydrol. Engl. Transl.* **7**, 53-60.

Jacob, D., and L. K. Shay, 2003: The role of oceanic mesoscale features on the tropical cyclone induced mixed layer response: A case study. *J. Geophys. Res.*

Jones, S. C., 1995: The evolution of vortices in vertical shear. I. Initially barotropic vortices. *Quart. J. Roy. Meteor. Soc.*, **121,** 821-851.

Jones, S. C., 2000a: The evolution of vortices in vertical shear. II. Large-scale asymmetries. *Quart. J. Roy. Meteor. Soc.*, **126,** 3137-3160.

Jones, S. C., 2000b: The evolution of vortices in vertical shear. III. Baroclinic vortices. *Quart. J. Roy. Meteor. Soc.*, **126,** 3161-3186.

Jones, S. C., 2003: The dynamics of tropical cyclones in vertical shear and of their extra-tropical transition. Habilitation thesis, University of Munich. Obtainable from: Meteorological Institute, University of Munich, Theresienstr. 37, 80333 Munich, Germany

Jordan, C. L., 1957: Mean soundings for the West Indies area. *J. Meteor.*, **15,** 91-97.

Kato, H. and O. M. Phillips, 1969: On the penetration of a turbulent layer into stratified fluid. *J. Fliud Mech.*, **37**, 643-655.

Kraus, E. B., and J. S. Turner, 1967: A one-dimensional of the seasonal thermocline. 2. The general theory and its consequences. *Tellus*, **19**, 98-105.

Niller, P. P., and E. B. Kraus, 1977: One-dimensional models of the upper ocean. *Modelling and Prediction of the Upper Layer of the Ocean*, E. B. Kraus, Ed., Pergamon Press, 143-172.

Phillips, O. M., 1977: Entrainment. *Modelling and prediction of the upper layers of the ocean, E.B.Kraus, Ed. Pergamon Press*, 285pp.

Price, J. F., C. N. K. Mooers, and J. C. V. Leer, 1978: Observation and simulation of storm-induced mixed-layer deepening, *J. Atmos. Sci.*, **8**, 582-599.

Price, J. F., 1979: On the scaling of stress-driven entrainment experiments. *J. Fluid Mech.*, **90**, 509-529.

Price, J. F., 1981: Upper ocean response to a hurricane. 1981 *J. Phys. Oceanogr.*, **11**, 153-175.

Pollard, R. T., P. B. Rhines, and R. O. R. Y. Thompson, 1973: The deepening of the wind-mixed layer, *Geophys. Fluid Dyn.*, **4**, 381-404.

Schade, L. R., and K. A. Emanuel, 1999: The ocean's effect on the intensity of tropical cyclones: Results from a simple coupled atmosphere-ocean model. *J. Atmos. Sci.*, **56**, 642-651.

Shapiro, L. J., 1983: The asymmetric boundary layer flow under a translating hurricane. *J. Atmos. Sci.*, **40,** 1984-1998.

Shapiro, L. J., 1992: Hurricane vortex motion and evolution in a three-layer model.*J. Atmos. Sci.*, **49,** 140-153.

Shay, L. K., P. G. Black, A. J. Mariano, J. D. Hawkins and R. L. Elsbery, 1992: Upper ocean response to hurricane Gilbert. *J. Geophys. Res.* ,**C12,** 20277-20248.

Smith, R. K, 2003: A simple model of the hurricane boundary layer. *Quart. J. Roy. Meteor. Soc.*, **129,** 1007-1027.

Smith, R. K., W. Ulrich, and G. Dietachmayer, 1990: A numerical study of tropical cyclone motion using a barotropic model. Part I: The role of vortex asymmetries. *Quart. J. Roy. Meteor. Soc.*, **116,** 337-362.

Sutyrin, G. G., A. P. Khain, and E. A. Agrenich, 1979: Interaction of the boundary layers of the ocean and the atmosphere on the intensity of a moving tropical cyclone. *Meteor. Girol.*, **2,** 45-56.

Yano, J., and K. A. Emanuel, 1991: An improved model of the equatorial troposphere and its coupling with the stratosphere. *J. Atmos. Sci.*, **48,** 377-389.

Zhu H., and R. K. Smith, 2003: Effects of vertical differencing in a minimal hurricane model. *Quart. J. Roy. Meteor. Soc.,* **129,** 1051-1069.

Zhu H., R. K. Smith, and W. Ulrich, 2001: A minimal three-dimensional tropical cyclone model. *J. Atmos. Sci.*, **58,** 1924-1944.

Figure Caption

Fig. 1: A schematic of the coupled tropical cyclone - ocean model.

Fig. 2: SST deviation (unit: ^{o}C) from that at the initial time to 72 h in: (a) Expt. 2, and (b) Expt. 3. The inner core region of the cyclone is represented by the contour lines of surface wind speed exceeding 30 m s^{-1}. The hurricane centre at the initial time and at 72 h are indicated by the hurricane symbol. The origin of the x- and y- coordinates is at the initial vortex position.

Fig. 3: (a) The minimum surface pressure (unit: mb) and (b) the maximum boundary layer wind speed (unit: ms^{-1}) in the calculation with and without ocean coupling. The numbers on the curves refer to the experiment number in Table 1.

Fig. 4: The distribution of the total surface heat flux (unit: kWm^{-2}) at 72 h for Expts. 1, 2, and 3. The positive value is directed upward into the atmosphere. The hurricane centre at 72 h is indicated by the hurricane symbol and the core region is represented by the contour line of surface wind speed of 30 m s^{-1}. The units and origin of the x- and y- coordinates are the same as in Fig. 2.

Fig. 5: The comparison of azimuthal average of total heat flux (unit: kWm^{-2}) at 72 h in Expt. 1, 2, 3. The numbers on the curves refer to the experiment number in Table 1.

Fig. 6: The azimuthal average moist static energy (unit: $kJkg^{-1}$) at the top of the boundary layer (level-$3\frac{1}{2}$) in the calculations for Expts. 1, 2, and 3 at 72 h. The numbers on the curves refer to the experiment number in Table 1.

Fig. 7: Averaged vertical velocity (ω, unit: 10^{-3} mb s^{-1}) at level-$2\frac{1}{2}$ ($\sigma = 0.6$) during the time period 60 h to 72 h for the experiments (a) Expt. 1, (b) Expt. 2 and (c) Expt. 3. Value smaller than -5×10^{-4} mb s^{-1} are shaded to highlight the cores of maximum ascent. The units of the x, y coordinates are same as Fig. 2, and the values represent the distance from the vortex centre.

Fig. 8: Averaged divergence field (unit: 10^{-4} s^{-1}) during the time period of 60 h and 72 h for Expts. 1 (a,b), and Expt. 2 (c,d) at the level-4 (a,c) and level-3 (b,d). The units and origin of the x- and y- coordinates are the same as in Fig. 7.

Fig. 9: Averaged asymmetric value of potential temperature (unit: K) at the level-$2\frac{1}{2}$ during the time period of 60 h and 72 h for the Expt. 1 and 2. The units and origin of the x- and y-coordinates are the same as in Fig. 7.

Fig. 10: The 72 h storm tracks for Expts. 1 - 2 - Expt. 3. The storm positions at 12 h intervals are indicated by the experiment number.

TABLE 1. List of experiments described in this paper.

Experiment	Sensitivity experiment
1	Without ocean coupling and a uniform SST of 28°C
2	With ocean coupling model, the entrainment velocity is based on TEM
3	With ocean coupling model, the entrainment velocity is based on DIM

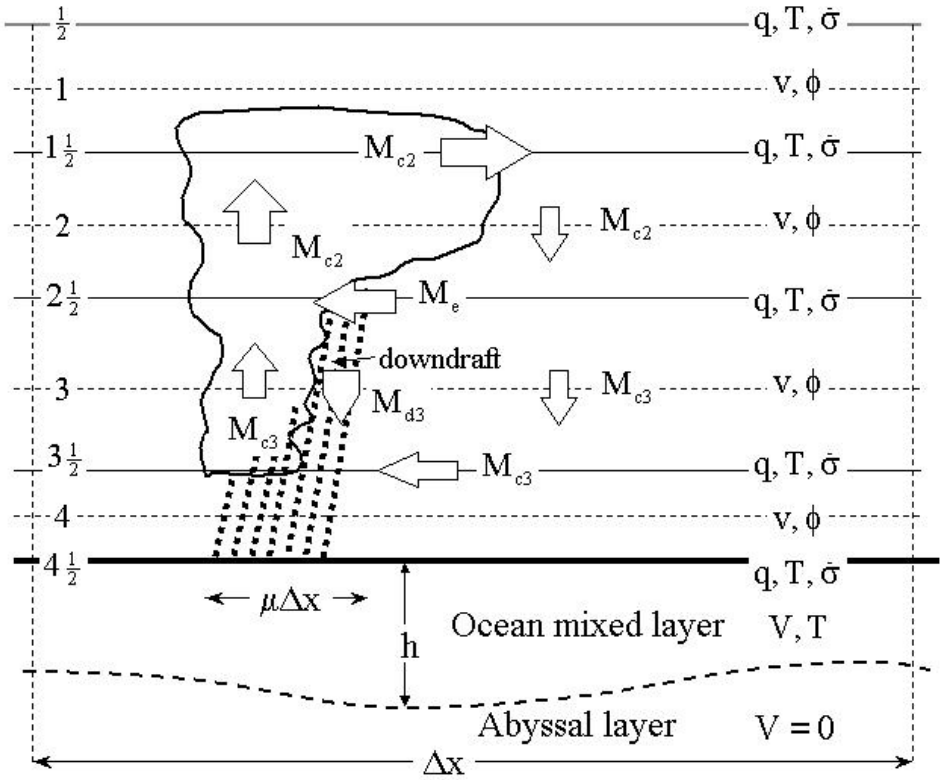

Figure 1.

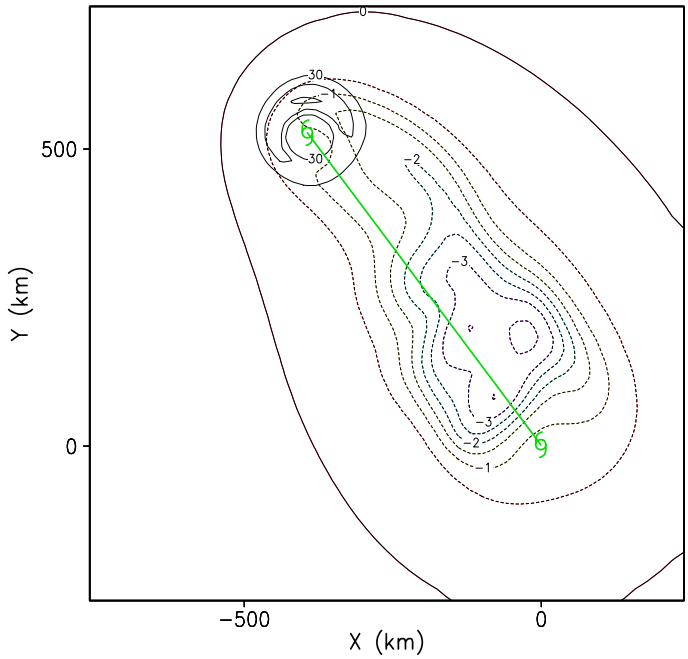

(a)

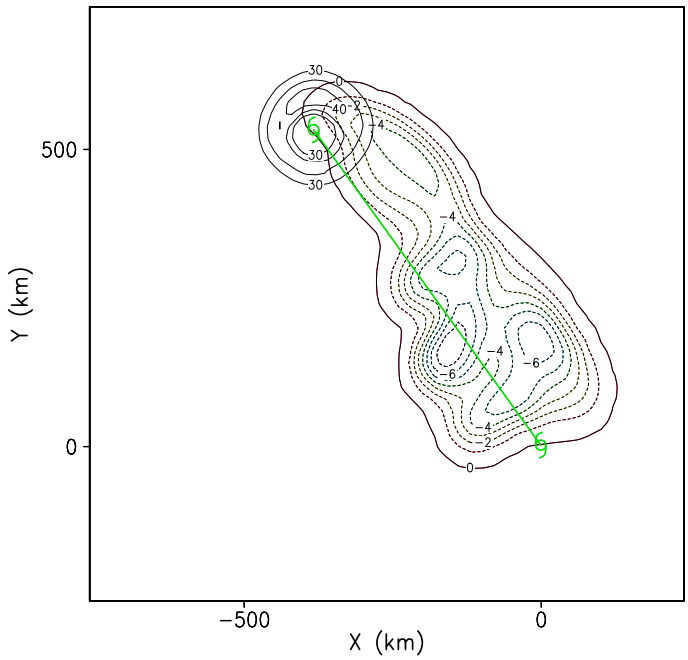

(b)

Figure 2.

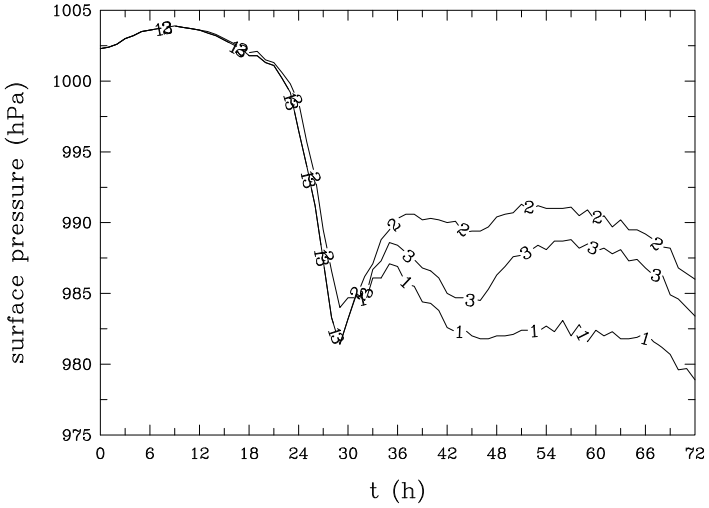
surface pressure (hPa)
1005
1000
995
990
985
980
975
0
6
12
18
24
30
36
42
48
54
60
66
72
t (h)

(a)

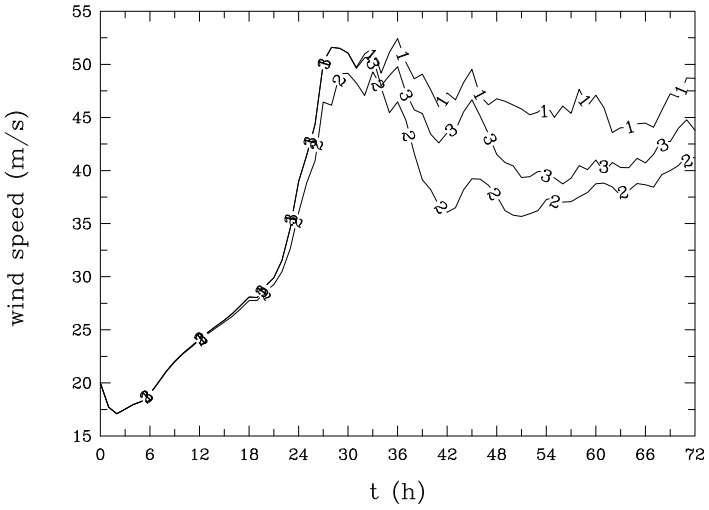
wind speed (m/s)
55
50
45
40
35
30
25
20
15
0
6
12
18
24
30
36
42
48
54
60
66
72
t (h)

(b)

Figure 3.

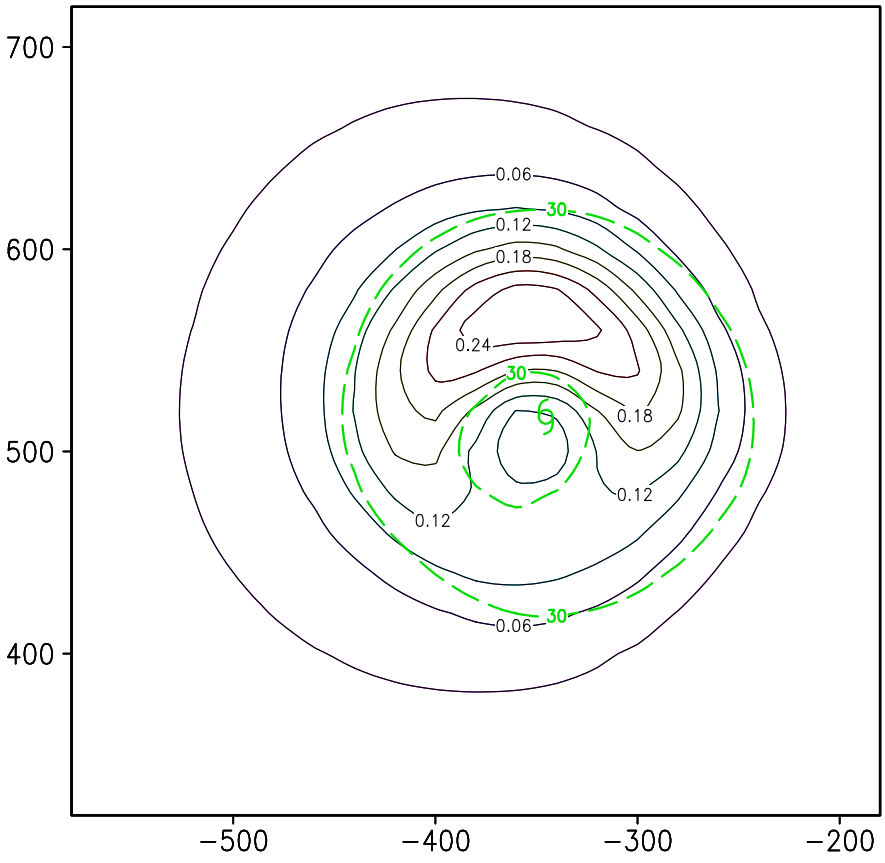
700
600
500
400
−500
−400
−300
−200
0.06
30
0.12
0.18
0.24
30
0.18
0.12
0.12
0.06
30

Fig. 4a

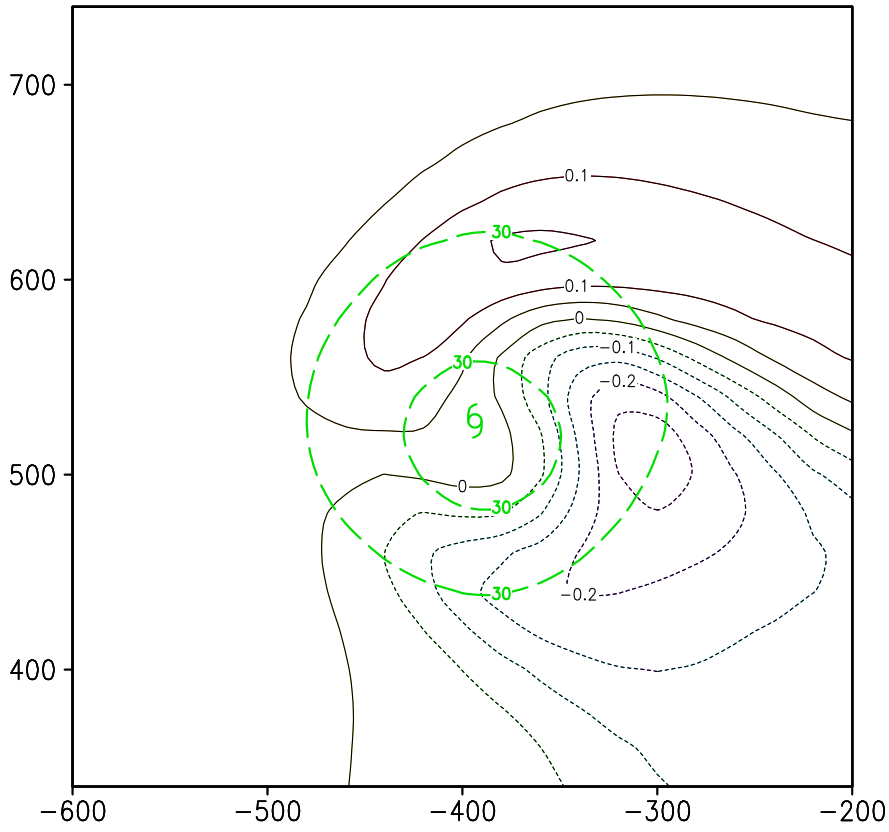

Fig. 4b

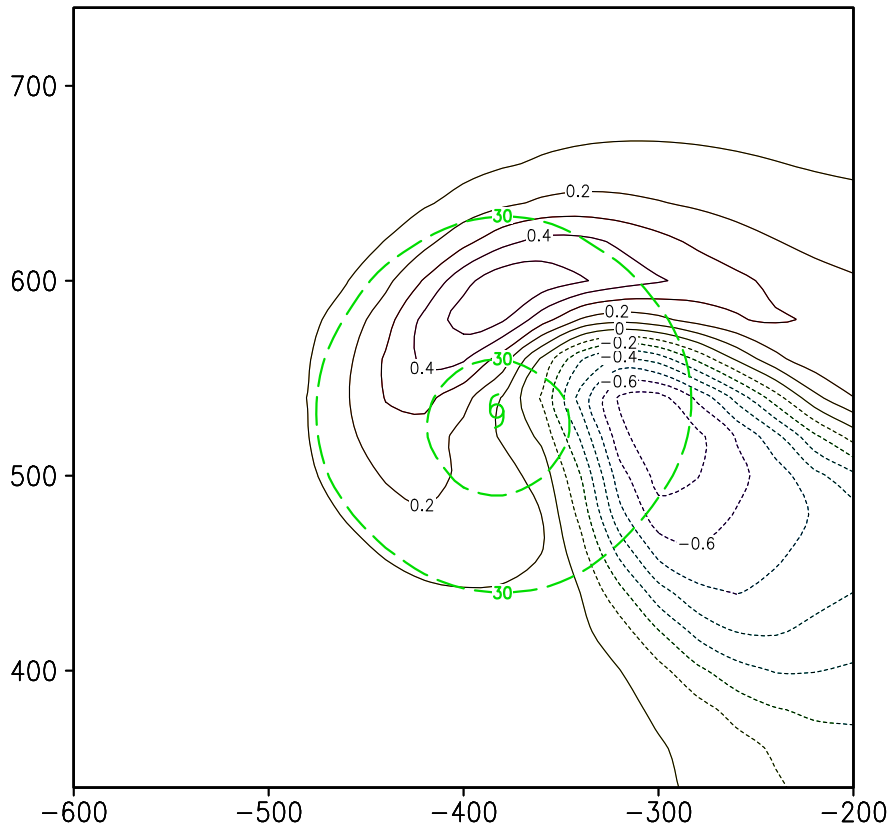

Fig. 4c

Figure 4.

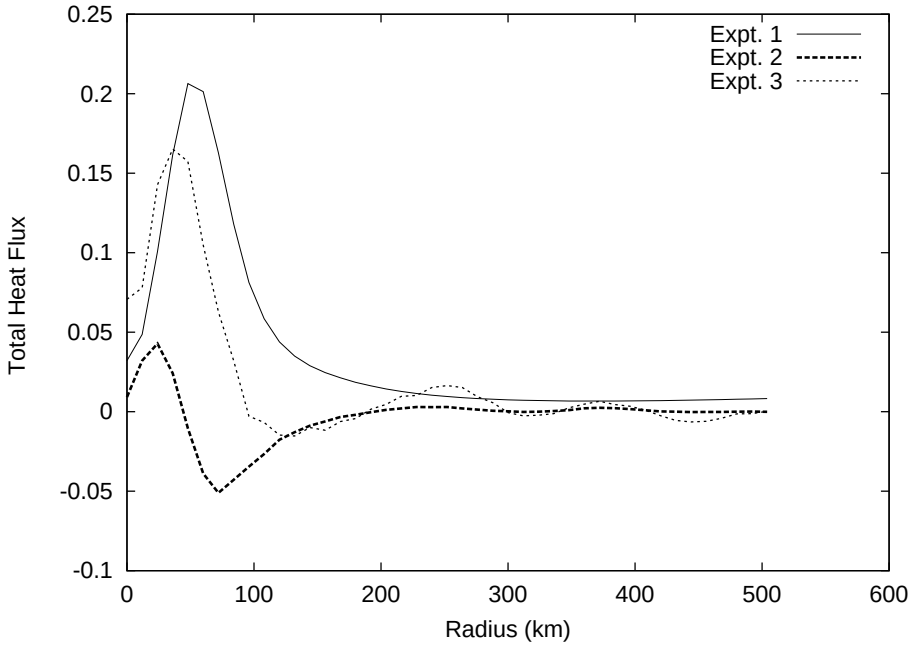

Figure 5.

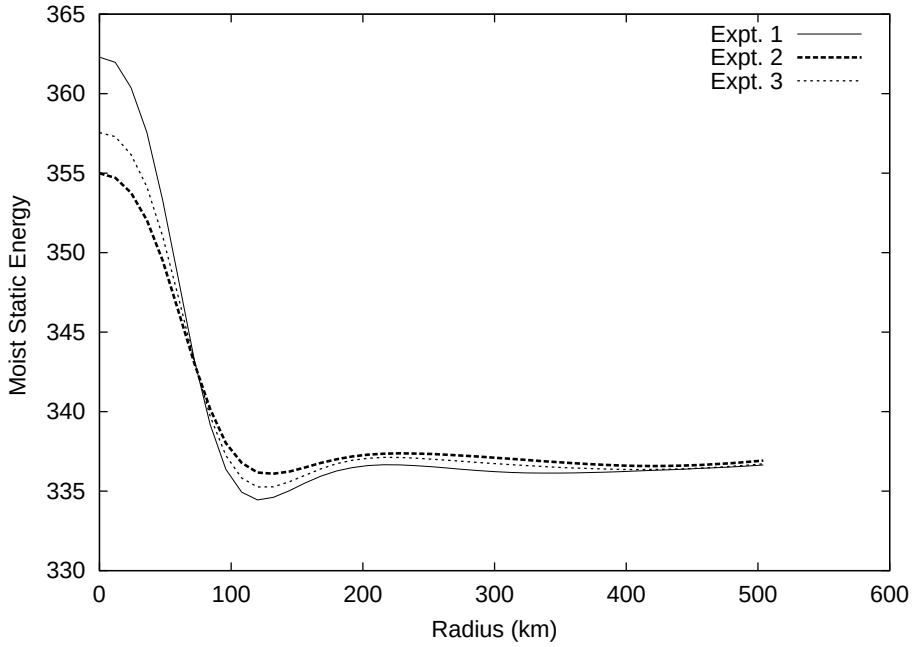

Figure 6.

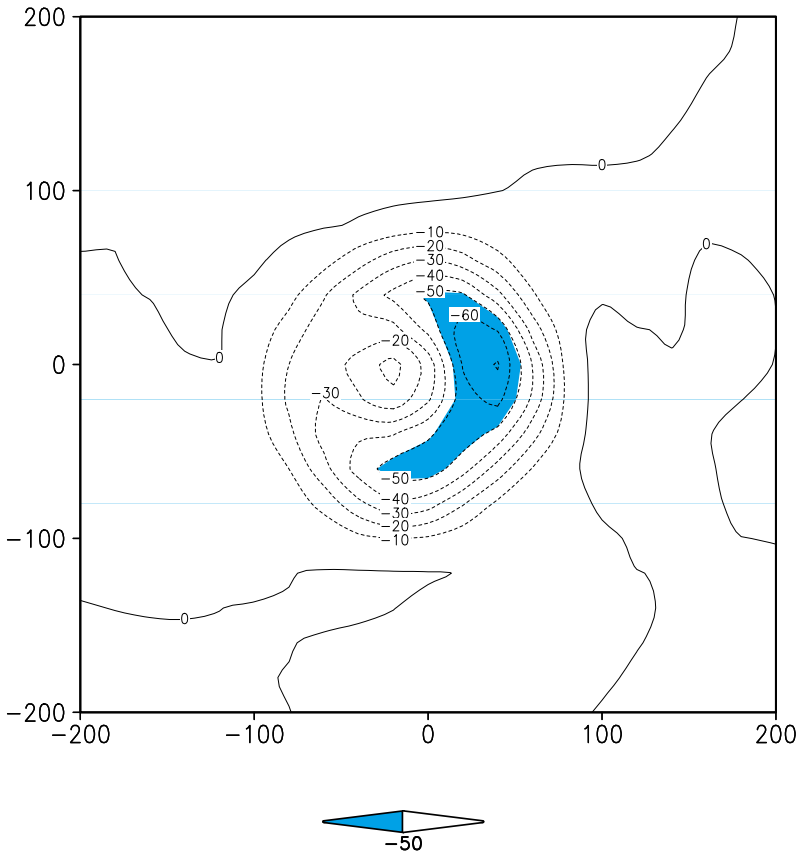

Fig. 7a

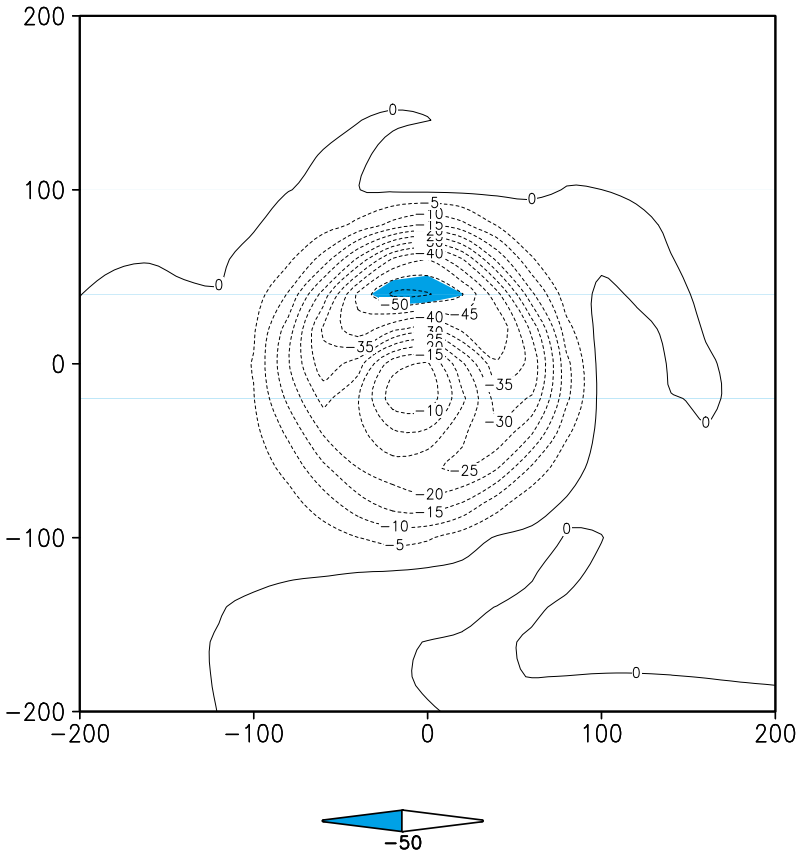

Fig. 7b

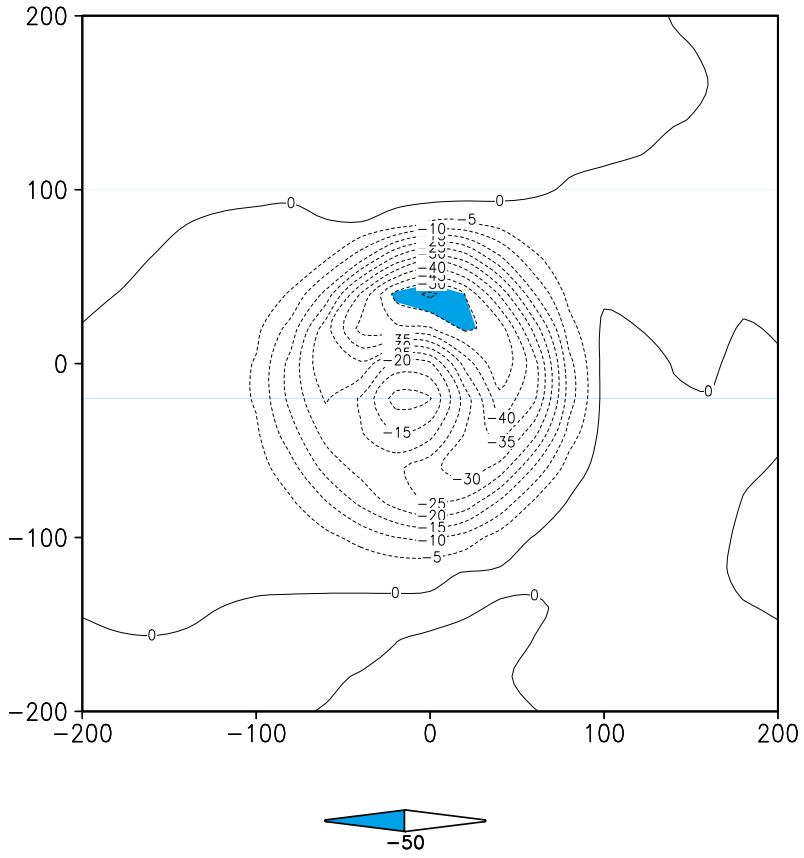

Fig. 7c

Figure 7.

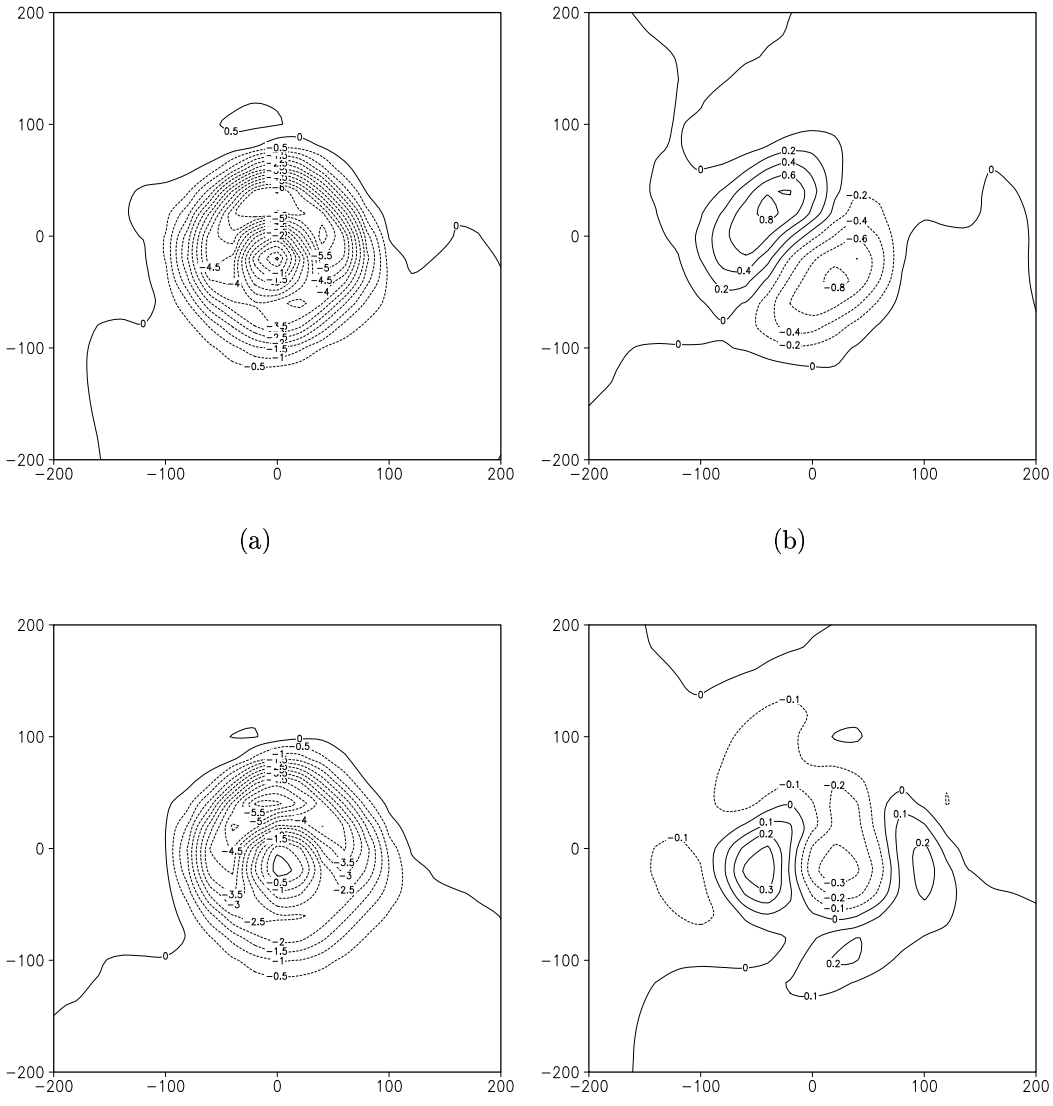

Figure 8.

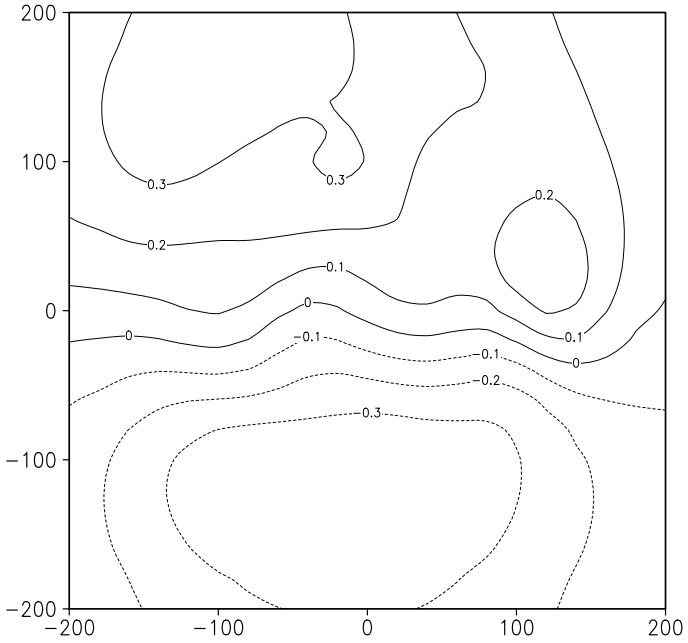
200
100
0
−100
−200
−200
−100
0
100
200
0.3
0.3
0.2
0.2
0.1
0
0.1
0
−0.1
0.1
0
−0.2
−0.3

(a)

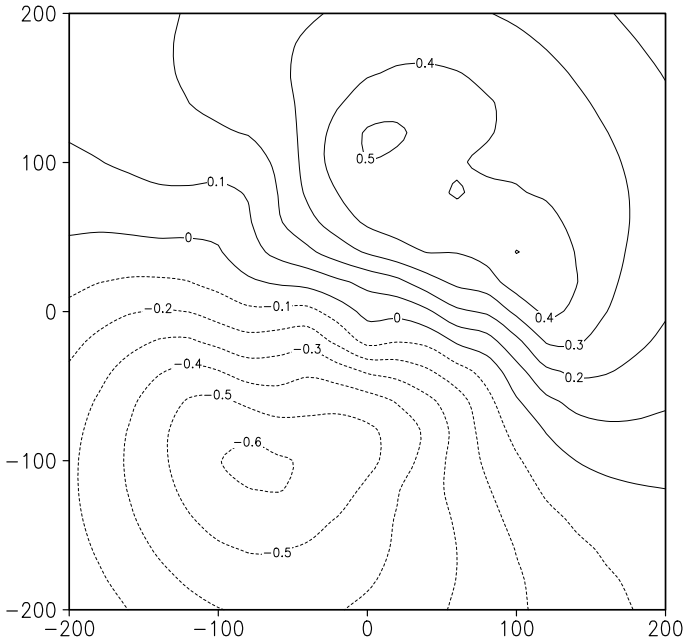
200
100
0
−100
−200
−200
−100
0
100
200
0.4
0.5
0.1
0
−0.2
−0.1
0
0.4
0.3
−0.3
0.2
−0.4
−0.5
−0.6
−0.5

(b)

Figure 9.

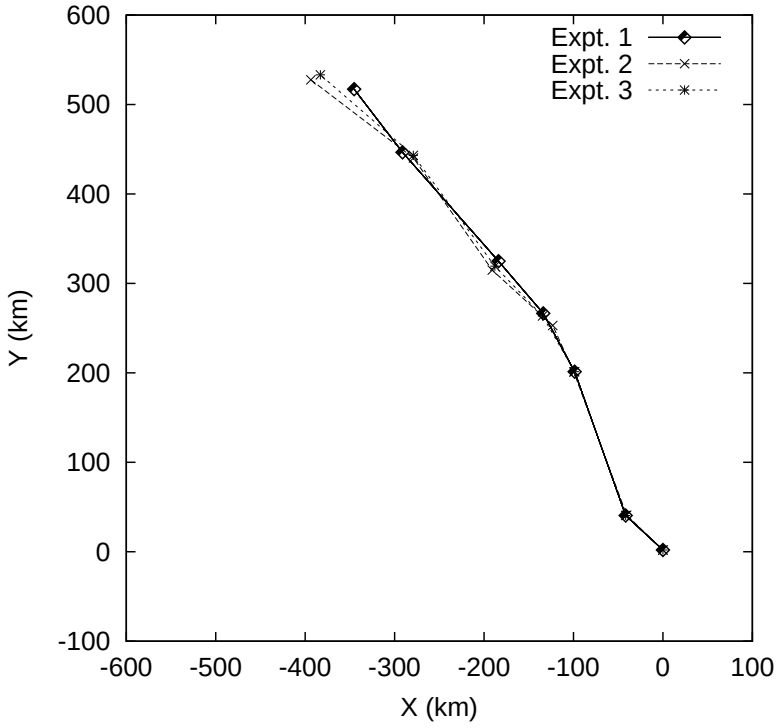
Expt. 1
Expt. 2
Expt. 3
600
500
400
300
200
100
0
-100
Y (km)
-600
-500
-400
-300
-200
-100
0
100
X (km)

Figure 10.